Sensors & Actuators: B. Chemical 371 (2022) 132459

Contents lists available at ScienceDirect

Sensors and Actuators: B. Chemical

journal homepage: www.elsevier.com/locate/snb

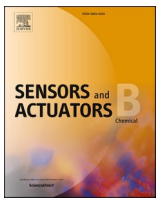

Impedimetric sensing of α-amino acids driven by micro-patterned 1,8-Diazafluoren-9-one into titania- boron- doped maze-like nanocarbons

Mattia Pierpaoli [a,b,*], Aneta Lewkowicz [c,**], Bartłomiej Dec [b], Małgorzata Nadolska [d], Robert Bogdanowicz [b]

[a] Advanced Materials Center, Gdańsk University of Technology, ul. Narutowicza 11/12, Gdańsk 80-233, Poland
[b] Faculty of Electronics, Telecommunications and Informatics, Gdańsk University of Technology, 11/12 Gabriela Narutowicza Street, Gdańsk 80-233, Poland
[c] Faculty of Mathematics, Physics and Informatics, University of Gdańsk, Wita Stwosza 57, Gdańsk 80-308, Poland
[d] Faculty of Applied Physics and Mathematics, Gdańsk University of Technology, 11/12 Gabriela Narutowicza Street, Gdańsk 80-233, Poland

ARTICLE INFO

Keywords:
Carbon nanowall
Biosensor
Chemical vapour deposition
Electrochemical detection
Glycine

ABSTRACT

The development of impedimetric, non-faradaic label-free sensors for the detection of α-amino acids constitutes a trailblazing technology for the fast and inexpensive quantification of such biomarkers. Since α-amino acids, such as glycine and sarcosine, are basic constituents in biological processes, a variation in their concentration may be an indicator of cardiovascular diseases and metabolic disorders or neurological conditions. The unique properties, including maze-like porosity along with excellent electron transfer behavior, make boron-doped carbon nanowalls (BCNW) an ideal transducer for electrochemical sensing. In order to realize a non-faradaic impedimetric sensor for the detection of α-amino acids, 1,8-diazafluoren-9-one (DFO), a fluorophore commonly used in forensic science, was dispersed into Ti-sol precursor and deposited over a BCNW substrate by spin-coating. Data mining tools have been applied to the raw impedimetric data to directly predict the glycine concentration and to support the underlying material-interface interaction. The developed sensor revealed high selectivity and reproducibility toward glycine and other α-amino acids (phenylamine, sarcosine and tryptophan) and no selectivity toward β-alanine, γ-aminobutyric acid or taurine. The application of density-functional theory (DFT) studies supported the higher affinity with the highest adsorption energy for the reaction product of DFO with glycine. A detection limit of 51 nM was found for glycine.

1. Introduction

α-amino acids are considered to be powerful biomarkers, and for this reason, measuring any change in their concentration is a priority for fast and accurate diagnoses of cardiovascular diseases, metabolic disorders and neurological conditions [1]. Namely, all amino acids of which proteins are made are alpha type, in which the amino group is bonded to the same carbon atom of the molecule where the carboxyl group is attached [2]. Amino acid ions are typically amphiprotic individuals. Their ammonium groups are acidic protonators, and their carboxyl groups are alkaline protonators. The side chains also play an important role and can also participate in proteolytic reactions with water [2]. Sarcosine has been indicated as a potential biomarker in the blood and urine of early-stage prostate cancer tumors [3,4], while altered plasma glycine levels have been related to obesity [5], diabetes [5], nonketotic hyperglycinemia [6] and gout [7]. The standard method to detect amino acids is based on liquid chromatography and capillary electrophoresis associated with mass spectrometry (LC–MS and CE-MS) [8]. Electrochemical detection of proteins and amino acids, by direct redox reactions or oxidation/reduction of side chains of their amino acid residues, benefits from the simplicity, low cost, speed, and potential for miniaturization, thereby making it particularly suitable for point-of-care applications. Since the pioneering work of Brabec and Mornstein [9], where the electrochemical oxidation of α-amino acids (tyrosine, tryptophan, histidine, cystine, cysteine and methionine) was investigated on graphitic electrodes, it was found that only on carbon electrodes, tryptophan, tyrosine, and cysteine exhibit a well-defined oxidation peak. While voltammetric or amperometric techniques have been widely employed for amino acid detection, a major drawback is the low level of oxidation current. While it was generally accepted that only a few amino

* Corresponding author at: Advanced Materials Center, Gdańsk University of Technology, ul. Narutowicza 11/12, Gdańsk 80-233, Poland.
** Corresponding author.
E-mail addresses: mattia.pierpaoli@pg.edu.pl (M. Pierpaoli), aneta.lewkowicz@ug.edu.pl (A. Lewkowicz).

https://doi.org/10.1016/j.snb.2022.132459
Received 11 March 2022; Received in revised form 1 August 2022; Accepted 1 August 2022
Available online 9 August 2022

acids could be oxidized on carbon electrodes, Suprun and co-workers [10] employed Prussian Blue to catalyze the specific electrochemical oxidation to pursue the oxidation of most amino acids. While a chromatographic analysis may differentiate between different amino acids, it may fail to discriminate between those with similar molecular weights (such as sarcosine and alanine). For this reason, the development of a simple, low-cost sensor for the detection of a specific type of biomarkers may represent an opportunity for the early detection of cancer and other pathologies [11,12].

Carbon nanowalls (CNWs), among various carbon-based nanomaterials, are open bounded, vertically-oriented few-layer graphene sheets which possess extraordinary properties [13]. For this reason, CNWs have attracted attention due to their tunable bandgap, high conductivity, high mechanical robustness, high light absorption, high chemical inertness, and large specific surface area. To achieve a particular morphology and characteristic, it is possible to vary the synthesis parameters, such as heating temperature, plasma intensity, substrate, deposition time, and gas precursor ratios, and by introducing dopants [14]. Widely adopted electrochemical techniques for the detection of different biomolecules rely on the addition of additional redox probes, which oxidation and reduction make it possible to measure the signal response on a specific electrode.

In contrast to the previously mentioned technique, non-faradaic electrochemical impedance spectroscopy can detect the capacitance changes of the electrode-solution interaction, without the need for a redox molecule. When considering the electrochemical cell, a TiO_2 film constitutes a thin dielectric layer in the electrolyte/dielectric/semiconductor structure, so that the electrical behavior is dominated both by the capacitance of the dielectric layer and the charge layer. In this work, in order to make this layer sensitive to the target amino acids, 1,8-diaza-fluoren-9-one (DFO), a fluorescent probe used in forensic science to detect latent fingerprints on various materials, was entrapped within a gel. In previous works, the ability of DFO to form a photoluminescent product with α-amino acids was explored [15–17]. Electrochemical impedance spectroscopy (EIS) is a powerful electrochemical technique for studying the electrode–solution interface by means of applying a small-amplitude alternating voltage signal to the sensing electrode, with the frequency varying over a wide interval. Conventionally, the resulting impedance spectrum undergoes an arbitrary fitting with an equivalent electrical circuit (EEC), to estimate and extract the valuable EEC parameters. On the other hand, the choice of an EEC to fit real electrochemical systems is arbitrary; while using a single time-constant EEC may lead to an oversimplification of the system, resulting in a loss of information, increasing the complexity of the EEC requires justification in terms of physical meaning. For these reasons, an alternative way of dealing with EIS data should be investigated. While the use of principal component analysis (PCA) on singular-value decomposition (SVD)-treated complex impedance data was already introduced in 2009 by Geladi et al. [18], the application of partial least-squares (PLS) regression was only recently studied. Rodriguez et al. found the mean-centered complex impedance to be preferable rather than using only the real or imaginary parts of the complex impedance, or the absolute impedance or the phase angle in quantifying the ferrocyanide, hydroquinone, and catechol concentration [19]. Moreover, the application of multivariate data analysis techniques allows the direct analyte concentration to be determined without the subjective assumptions of an EEC.

The aim of this study is to develop and investigate a novel electrochemical non-faradaic label-free impedimetric biosensor for the detection and quantification of α-amino acids. The ability of specific amino acids to selectively react with a DFO@TiO_2 film was exploited as the sensitive layer of a label-free impedimetric biosensor. Boron-doped CNWs (BCNWs) were grown over a different substrate and used as a transducer for the fabrication of the biosensor, on which the DFO@TiO_2 layer was spin-coated, in order to benefit from their maze-like geometry and superior electrical properties. The selective reaction of DFO with α-amino acids and the subsequent complex formation led to a capacitance change which was monitored by the impedance spectroscopy technique. Moreover, PLS regression was applied to the electrochemical spectral data to better understand the underlying relations without the intermediate step of fitting to an EEC. The Limit of Detection (LoD) for glycine was determined to be equal to 51 nM and a comparable sensitivity among different selected α-amino acids was determined (Tryptophan, Phenylalanine, Sarcosine). The results may pave the way for the development of P-o-C devices for the detection and quantification of α-amino acids by employing an inexpensive and simple technique.

2. Experimental section

2.1. Synthesis of boron-doped carbon nanowalls

Two different substrates were used to grow BCNWs. A crystalline conductive substrate, consisting of a 1 × 1 cm^2 (100) oriented silicon, was seeded by sonication in a water-based diamond slurry. BCNWs were grown by an MPECVD system (SEKI Technotron AX5400S, Japan) using a gas mixture of H_2, CH_4, N_2, and B_2H_6, microwave power of 1.3 kW and pressure of 10^{-4} Torr inside the chamber, for 6 h [14] (sBCNW). The substrate holder was heated at 700 °C. Using the same process parameters, an amorphous, not-conductive, and optically transparent quartz was used to grow BCNWs for 10 min (qBCNW) after a 10-min pretreatment in H_2-rich plasma. A preliminary investigation aimed at finding the optimal BCNW thickness for the qBCNW sample was conducted and the results are reported in Fig. S1. Four sets of samples were prepared and tested in triplicates. A detailed characterization of the MPECVD-synthesized BCNW can be found in our previous studies [20,21].

2.2. Functionalization with DFO@TiO_2

Applied reagents and luminophores were spectrally pure. DFO was purchased from Aldrich (Germany). Titanium (IV) isopropoxide (TTIP), Triton X-100, and pentane-2,4-dione, were also purchased from Aldrich (Germany). Propane-2-ol, ethanol, and hydrochloric acid were purchased from POCh (Poland). Deionized (DI) water was produced by a Hydrolab deionizer. The luminophore – 1,8-diaza-fluoren-9-one (DFO) – was incorporated in situ into the sol of the Ti-sol with an alcoholic solution at room temperature and under atmospheric pressure at a concentration of 10 mM. The DFO loading amount was chosen to avoid the formation of aggregates [22]. Initially, films were prepared with a gelation time (defined as the time measured from the moment the catalyst was added to the sol until its deposition by spin coating) of 2 h. Thin films were prepared by the spin coating technique: 25 μL of the Ti-sol was drop-casted onto the BCNW sample and centrifuged at a speed of 2000 rpm for 60 s. The electrodes were then dried in a vacuum oven at 80 °C, − 60 kPa, for 2 h.

2.3. Sample characterization

Scanning electron microscopy (SEM) was performed by a Phenom XL microscope, using a 10-kV beam accelerating voltage, working in high vacuum mode and with a secondary electron detector (SED). The attenuated total reflection Fourier transformed infrared (ATR-FTIR) spectra were collected on a Perkin Elmer Frontier spectrophotometer equipped with a ZnSe crystal. Spectra were recorded in the range of 550–4000 cm^{-1}, with 5 scans and a resolution of 0.5 cm^{-1}.

2.4. Sample collection and preparation

All electrochemical tests were conducted in spiked samples, containing phosphate solution (PS, 8.733 g of K_2HPO_4 and 125 μL of 85 % H_3PO_4 were dissolved in a 500-mL volumetric flask using distilled water).

Saliva is an ideal diagnostic medium to provide molecular biomarkers for a variety of oral and systemic diseases and conditions [23]. Saliva sample collection was performed on one healthy male volunteer who refrained from eating, drinking and oral hygiene procedures (for at least 1 h prior to the collection). The volunteer was given drinking water and asked to rinse well his mouth. 5 min after, the volunteer was asked to spit into a 50 mL sterile tube, until 5 mL of whole saliva (WS) was collected. WS was diluted in PB solution in the ratio of 1:50, spiked with glycine, and stirred using a vortex mixer.

In addition to spiked WS samples, the electrode has been tested also in synthetic urine (SU) samples. The composition for SU has been taken from the study of Brooks and Keevil [24] with modification and it is reported in Table S1. Before analysis, SU was diluted with glycine-spiked solutions in the ratio of 1:1.

2.5. Electrochemical measurements

Cyclic voltammetry (CV) was performed to evaluate the electrochemical properties of the different composites under an argon atmosphere, using a three-electrode system. The CV measurements were conducted in 5 mM $Fe[(CN)_6]^{3-/4-}$ (1:1) in 0.5 M of Na_2SO_4 solution with an applied scan rate equal to 100 mV s^{-1}. Non-faradaic EIS is a powerful technique to detect minimal changes at the electrode-solution interface without the need of a redox molecule. The functionalized BCNW electrode, a platinum wire and an Ag wire coated with AgCl were used as the working electrode (WE), auxiliary electrode (AE) and reference electrode (RE), respectively. The EIS was performed in the frequency range from 200 kHz to 20 mHz, with an amplitude of 20 mV at open circuit potential, after a fixed 10 min rest period for reaching equilibrium. Staircase potentio electrochemical impedance spectroscopy (SPEIS) was performed at the − 0.2, 0, + 0.2, + 0.4, + 0.6 V potential steps, in the frequency range from 1 MHz to 10 mHz, with an amplitude of 20 mV. From the SPEIS, capacitance values were calculated from the imaginary component of the impedance (Z"), at the frequency (*f*) of 25 mHz, according to (1):

$$C_s = -\frac{1}{2\pi f Z''} \quad (1)$$

All techniques were performed using a potentiostat/galvanostat (VMP-300, Bio-Logic, France). The coefficient of determination (R^2), sensitivity (slope of the linear regression in the concentration-capacitance plot), and LoD, were calculated. Due to the logarithmic nature of the correlation between the analyte concentration and the CPE equivalent capacitance, firstly, the limit of blank (LoB) was first estimated by substituting the values of capacitance found for PS-only into the linear calibration.

$$\mathrm{LoB} = \mathrm{mean}_{\mathrm{blank}} + 1.645(\mathrm{SD}_{\mathrm{blank}}) \quad (2)$$

Then, the LoD was calculated by utilizing both the measured LoB and test replicates of the sample known to contain the lowest analyte concentration [25]:

$$\mathrm{LoD} = \mathrm{LoB} + 1.645\left(\mathrm{SD}_{\mathrm{lowest\_concentration\_sample}}\right) \quad (3)$$

2.6. Partial least squares regression of the electrochemical dataset

PLS regression is a multivariate statistical technique that can predict a dependent variable from a set of independent variables (i.e., predictors) by attempting to maximize the covariance between the matrix with predictors and matrix with responses, rather than the variables themselves. PLS was performed on the EIS dataset, in which each observation of the predictor matrix is one experiment, represented by the values |Z| and phase(Z), recorded at 35 frequencies, resulting in a 18 × 70 dataset, and the response matrix is a 18 × 1 vector reporting the log-transformed glycine concentration. The EIS performed in the presence of PS-only was used to estimate the LoD, by using the PLS model to predict the equivalent concentration. The LoD was then calculated using (2) and (3). PLS analysis was performed using the mdatools package [26] in R [27]. An important assumption in model development is choosing the proper number of PLS components; while increasing their number may lead to a higher coefficient of determination, the added variables may divert attention from the main independent descriptors. For this reason, the number of optimal components was initially determined by randomization tests.

2.7. Adsorption simulation of DFO and its derivatives

Molecular dynamics (MD) calculations were conducted to investigate the interactions of DFO-based complexes with the TiO_2 matrix during the detection of α-Amino Acids. The Atomistix ToolKit (ATK) QuantumWise package [28] was utilized to perform the calculations of adsorption energies by means of ATK – ReaxFF (Reactive Force Field), which can be used to study the reactive system of TiO_2, DFO and glycine. The titania matrix was considered as nanocrystalline rutile (110) in agreement with prior studies [15]. The periodic boundary cell was utilized with sizes 12 Å x 20 Å x 46 Å. The DFO, glycine and their derivative similar to ninhydrin were taken from the ATK library database. The Quantumwise ATK Classical optimization was performed for all of the designed atomic models. The following parameters were applied: ReaxFF-CHO-2008 [29,30], Force tolerance: 0.01 eV/Å, and Stress tolerance: 0.1 GPa with a step size of 0.01 Å. The cost-effective LBFGS optimization algorithm was configured to limit the amount of computer memory used. It is the Broyden-Fletcher-Goldfrab-Shanno (BFGS) algorithm from the quasi-Newton family. Finally, the models were equilibrated at RT for 10,000 steps and then simulated for 1 ns in an aqueous environment.

3. Results and discussion

The procedure for preparing the nanostructured electrode can be divided into three main steps, namely substrate pretreatment, BCNW growth and functionalization and is schematized in Fig. 1.

3.1. Characterization of the nanoarchitectured heterostructure

The different heterostructures were characterized before and after the application by spin coating of the Ti-sol. Fig. 2a,b show SEM micrographs of the BCNW grown on quartz (qBCNW) and Si (sBCNW) substrates, at the same boron-doping level, for 10 min and 6 h, respectively. It is possible to observe, including from the magnification inserts, the different morphology, in terms of wall density and wall length, due both to the different process duration and substrate crystalline structure. In particular, for qBCNW, the wall lengths are shorter, resulting in a more dense wall morphology.

The subsequent deposition of the Ti-layer by spin coating led to the creation of localized defects due to the agglomeration and subsequent evaporation of Triton X-100 micelles in a different manner for the two different substrates Fig. 2(c,d), leading to the formation of micrometer-sized patterns. Indeed, it is possible to observe from the EDX analysis (performed on the bare Si substrate, without BCNW in order to distinguish the TiO_2-matrix from the substrate) that these areas have convex shapes, are carbon-rich (Fig. S2) and thinner, which may partially expose the maze-like BCNW structure in direct contact with the electrolyte. The defect boundaries originating from the micelle formation are characterized by a high concentration of Ti and O, which is in agreement with the fluorescence microscopy pictures from our previous study [16], in which DFO is mainly present. The average micelle size and agglomerates are dependent on the BCNW morphology, which strongly affects the Ti-sol coating. For the qBCNW substrate, the craters are circle-shaped and with a diameter on the order of few tens of micrometers, Fig. 2(c), while for the sBCNW substrate, the agglomeration is more evident, resulting in a more dense island-like morphology Fig. 2

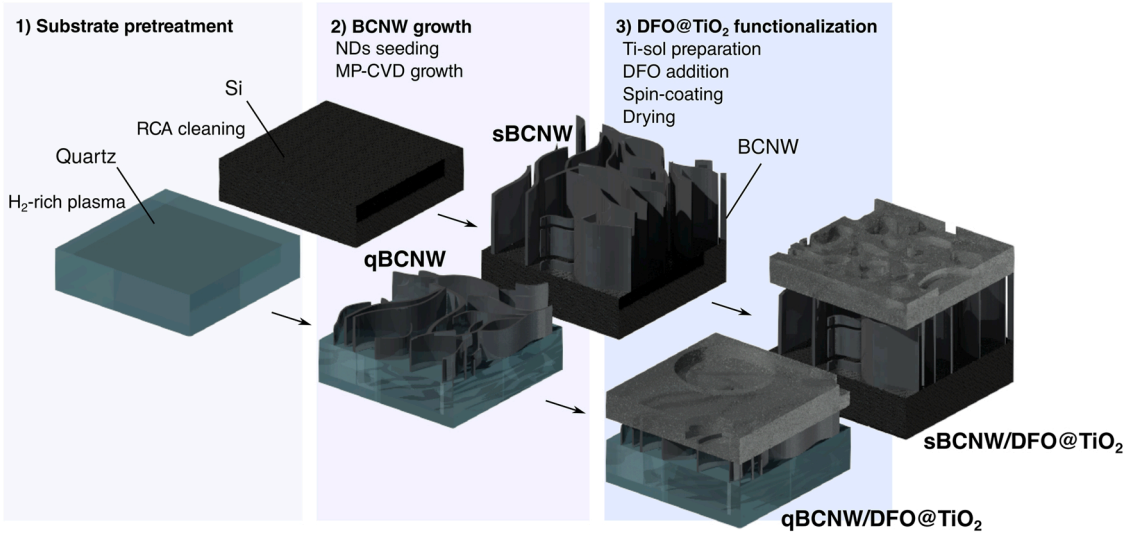

Fig. 1. (a) Schematic of the qBCNW/DFO@TiO2 electrode implementation. The qBCNW/DFO@TiO2 electrode followed the same scheme.

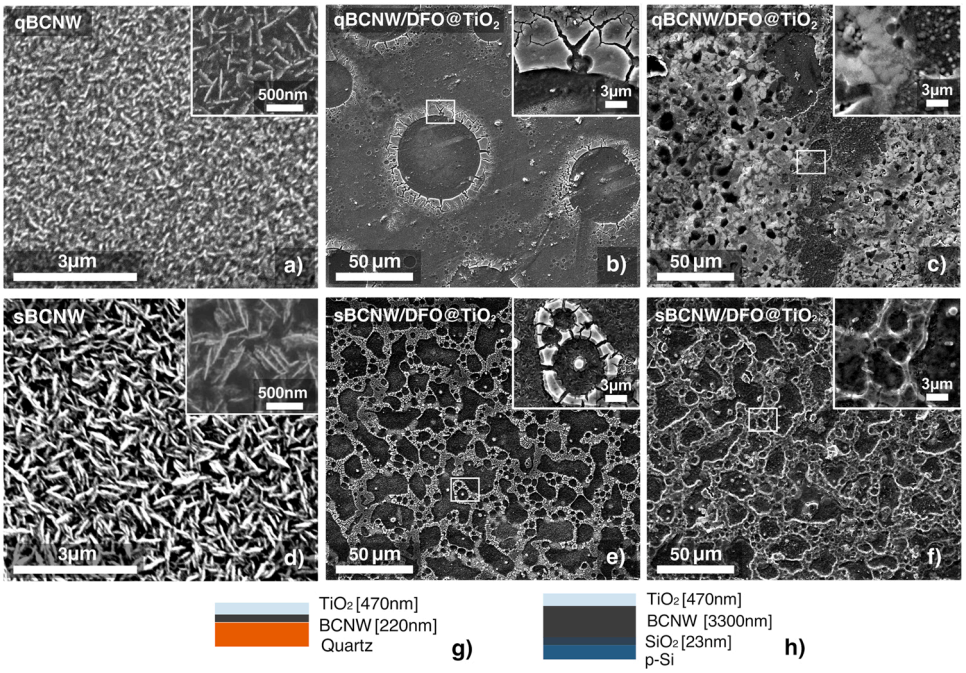

Fig. 2. SEM images of the (a,b) qBCNW and (d,e) sBCNW samples, before and (c,f) after the reaction with glycine. Insets are magnifications of the relative SEM. (g,h) Schematic description of the sample cross-section; thicknesses were measured by SEM.

(e). It is evident from Fig. 2e,f that the upper coating reacts with glycine, resulting in a morphology change, while the BCNW are inert. The experimental evidence for the DFO incorporation into the TiO_2 layer is supported by Raman spectroscopy in Fig. S3. Estimated layer thicknesses are reported in Fig. 2g,h. FTIR analysis (Fig. S4) shows that the observed sample spectra are dominated by signals corresponding to the TiO_2 layer. Unfortunately, signals characteristic of DFO overlapped with the signals measured for the TiO_2 sample. However, slight broadening of the bands in the lower wavenumbers (below 1150 cm^{-1}) may be evidence for DFO, which exhibits strong absorption bands in this region. It can also be noted that the intensity of the band at 1580 cm^{-1} in the qCNW/DFO@TiO_2 spectrum increased significantly. This band can be attributed to the C═C stretching vibration and its increase confirms the presence of carbon nanowalls in the sample.

3.2. Electrochemical detection of glycine

3.2.1. EEC fitting

The equivalent electric circuit (EEC) used to fit the experimental data is a modified Randles circuit. The ionic resistance (R_s) and the charge transfer resistance (R_{ct}) are the two resistive elements, describing the effect of the solution and the electrode, respectively. A constant phase element (CPE) has been used to describe the non-ideal impedance of the solid/electrolyte interfaces. The impedance of CPE is defined as [31]:

$$Z_{CPE} = (Q(j\omega)^{\alpha})^{-1} \quad (4)$$

where Q is the *quasi*-capacitance, α is the homogeneity factor, which compensates for the deviation from an ideal capacitor (α = 1), ω is the angular frequency and *j* is the imaginary number. Since Q does not have

a physical meaning, and because α is close to unity (α > 0.9) the CPE behavior is close to that of a capacitance, thus the effective capacitance has been calculated as follows [32]:

$$C_{eff} = Q^{\frac{1}{\alpha}} \quad R_{ct}^{\frac{1-\alpha}{\alpha}} \tag{5}$$

Thus, the total capacitance (C_{tot}) can be considered as a combination of the electrical double layer (C_{DL}) and the space charge (C_S) capacitances, connected in series (1):

$$\frac{1}{C_{tot}} = \frac{1}{C_S} + \frac{1}{C_{DL}} \tag{6}$$

For this reason, the total capacitance is more sensitive to the changes of the smallest capacitance in the series. Fig. 3a,b shows the non-faradaic impedimetric response of the two electrodes at increasing glycine concentrations. A calibration curve based on the changes of the capacitance values, estimated by fitting the experimental values to the EEC, with the logarithmic concentrations of glycine in PS from 0.1 μM to 1 mM, is shown in Fig. 3c, together with the calculated regression equations. The sBCNW/DFO@TiO_2 electrode has double the sensitivity of the quartz counterparts, but with a higher LoD. This is due to the higher standard deviation of the replicates at the lowest concentration. To investigate the specificity of the DFO@TiO_2 layer toward different α-amino acids, the impedimetric responses of the two synthesized electrodes to different probe molecules were investigated. Interestingly, it is possible to observe a difference in the sensitivity (expressed in μF per decade) among different analytes and different substrates (evaluated for the 10^{-8}–10^{-3} M range). A comparable sensitivity was found among selected α-amino acids (Tryptophan, Phenylalanine, and Sarcosine), with the sBCNW/DFO@TiO_2 sensor, while, for β-Alanine, γ-Aminobutyric acid and Taurine, a weak correlation was found (Fig. 3d).

In the SPEIS, the frequency of 25 mHz was chosen for the impedance measurements to allow the formation of the electrical double layer. Since the double layer capacitance (C_{DL}) and the one due to the space charge region (C_s) are in series, the resultant is the sum of their reciprocal. However, as C_s is much smaller than C_{DL}, its contribution is negligible. Thus, C_s, for the different electrodes, were calculated according to (1), and the results are plotted in Fig. 4a,b.

A few things can be derived from Fig. 4: firstly, the capacitance values for sBCNW/DFO@TiO_2 are one-order of magnitude higher than the sBCNW/DFO@TiO_2 values, as well as for the difference between different Gly concentrations. Secondly, for both electrodes, the higher C_s correspond to when a negative bias (−0.2 V) is applied. Indeed, from the Nyquist impedance diagrams, the semicircle's diameter substantially increases with the increasing potential and Gly concentration (Fig. 4c,d), leading to a harsher path for the electrolyte to diffuse to the electrode, while the opposite trend is found with a negative potential applied to the electrode.

3.2.2. PLS model

To highlight potential outliers among the collected data, a PLS model with robust estimator of critical limits was initially employed; two and one EIS measurements were identified as outliers [33] and removed from the qBCNW/DFO@TiO_2 and sBCNW/DFO@TiO_2 datasets, respectively. Then, randomization tests were performed to retain only the most important components for the PLS regression models, using the function *randtest()* from the mdatools R package. For the qBCNW/DFO@TiO_2 and sBCNW/DFO@TiO_2 PLS models, three and four components were found to be optimal, respectively (Table S4). In order to improve the performance and simplify the model, only variables with VIP-scores (variables important for projection) higher than the chosen thresholds were selected (Fig. S7). Finally, two PLS models were created, and the plot with the predicted vs. measured (reference) y-values is reported in Fig. 5a,b, while in the insert the RMSE values are shown along with the model components.

While it is possible to observe that the LoD are one order of magnitude greater than the ones calculated with the EEC-fitted EIS data, the PLS has the benefit of highlighting the variable that most accounts for the model, as represented by the averaged regression coefficients, in Fig. 5c. In particular, for both electrodes, two regions of interest (ROI) for the phase(Z) are present: one at high frequencies (ROI1, 20–200 kHz) and one at lower ones (ROI2, 20–200 mHz). Interestingly, the regression coefficients in these ROIs have opposite signs. ROI2 can be linked to the increasing Cs with increasing Gly concentration, since it is known that with the increasing phase(Z), the EEC tends to a capacitive behavior, and while the phase angles in the diffusive part (ROI2) decrease with the increasing glycine concentration, the ones in the inductive/Ohmic part increase.

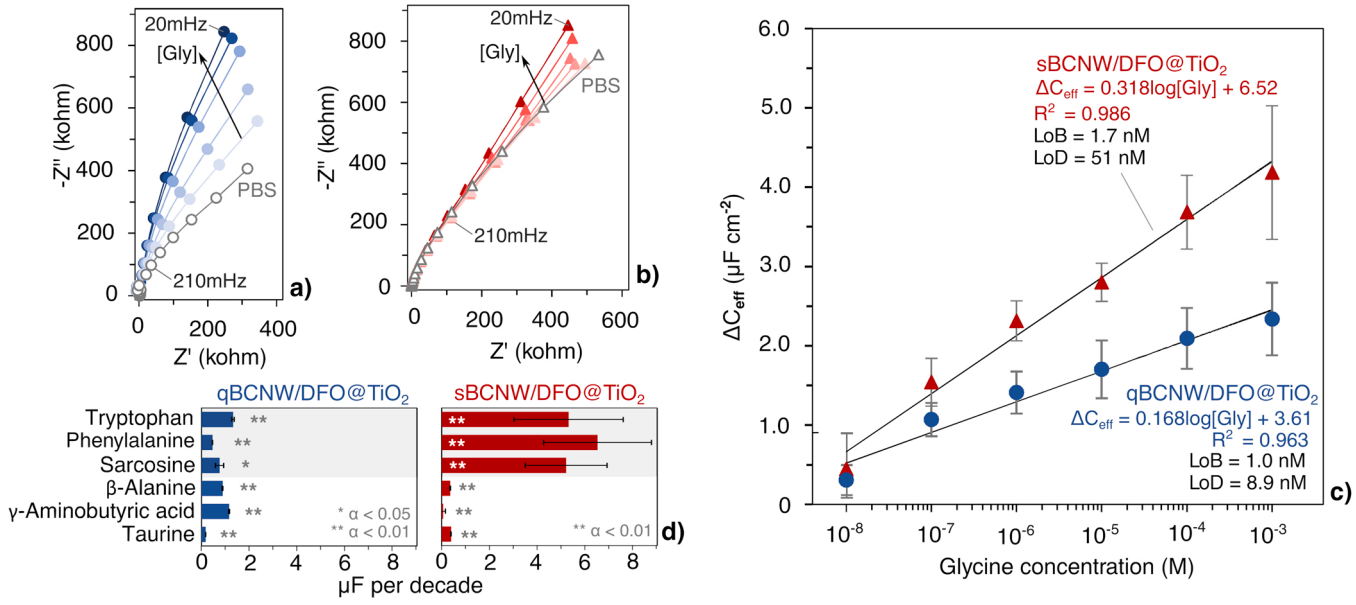

Fig. 3. Nyquist plots for the (a) qBCNW/DFO@TiO_2 and (b) sBCNW/DFO@TiO_2 electrodes at increasing glycine concentrations. (c) Correlation between the increase of capacitance and glycine concentration; error bars are the standard deviation (SD) of replicates calculated on three different electrodes. (d) qBCNW/DFO@TiO_2 and sBCNW/DFO@TiO_2 sensitivity toward other compounds.

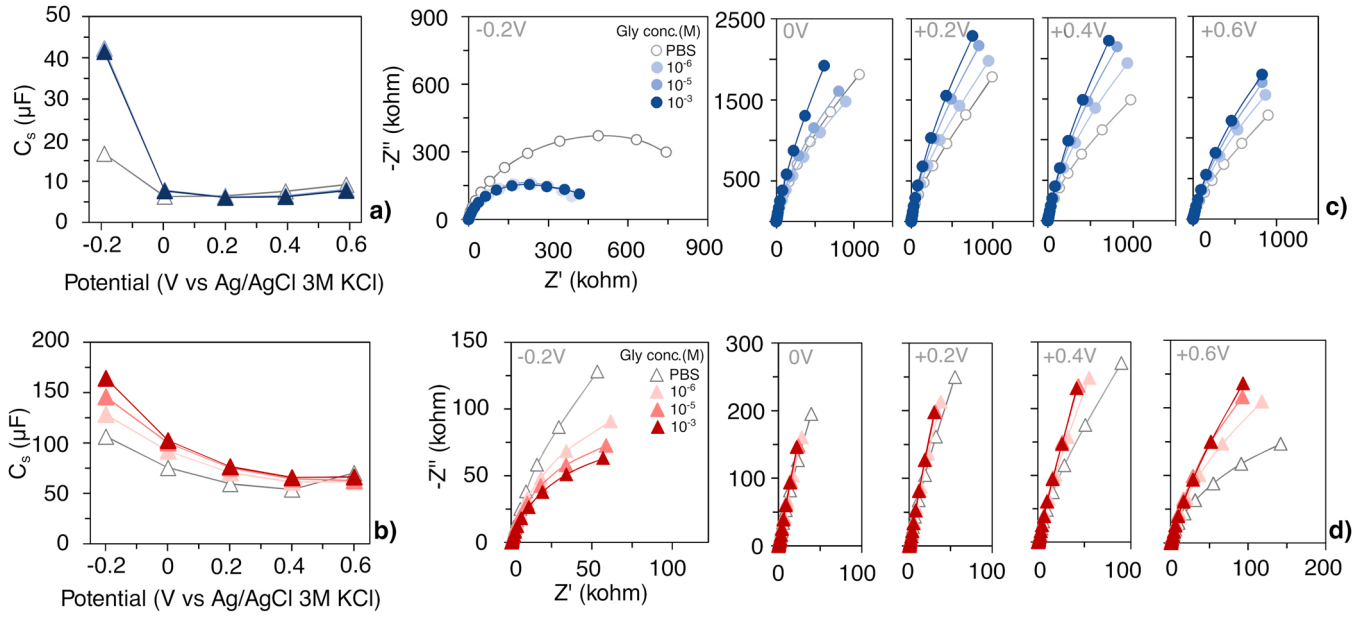

Fig. 4. (a,b) Space charge region capacitance evaluated as a function of the applied potential, and (c,d) Nyquist plots for the SPEIS results of the qBCNW/DFO@TiO_2 and sBCNW/DFO@TiO_2 electrodes.

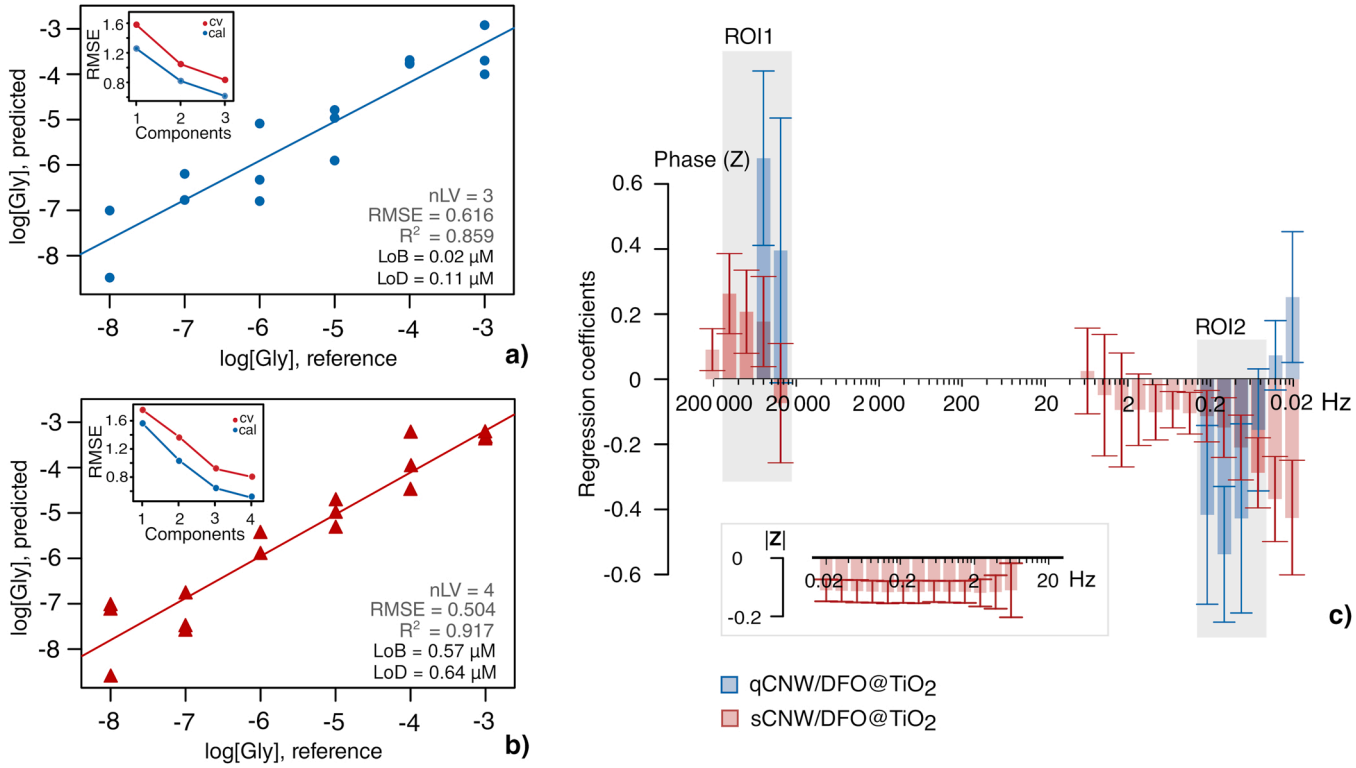

Fig. 5. (a,b) plot with measured glycine concentrations vs. predicted by the PLS model. (c) Plot comparing the regression coefficients for the qBCNW/DFO@TiO_2 and sBCNW/DFO@TiO_2 electrodes.

3.3. Real sample analysis

The developed impedimetric sensors qBCNW/DFO@TiO_2 and sBCNW/DFO@TiO_2 were applied to the determination of glycine in SU and WS. The results are reported in Table 1. The concentration of Gly, to prepare spiked samples, was chosen within the physiological ranges of glycine concentrations in different body fluids [4]. With the spiked WS, the recovery values ranged from 90.5 % to 94.7 % and 90.3–110.7 % for

Table 1
Determination of Gly in real samples.

Sample	Dilution	Gly added	Gly determined[a]	
			sBCNW/DFO@TiO_2	qBCNW/DFO@TiO_2
SU	1:1	1 μM	(1.2 ± 0.21) μM	(0.98 ± 0.06) μM
WS	1:50	0.5 μM	(0.47 ± 0.11) μM	(0.46 ± 0.01) μM

[a] The results are expressed as mean ± standard deviation (n = 3).

the qBCNW and sBCNW sensors, respectively. These results showed that the qBCNW/DFO@TiO_2 fabricated sensor has a better precision than the Si-based.

3.4. Selectivity and stability of the fabricated sensor

Selectivity is considered a critical factor in evaluating the performance of the developed sensor. To assess the impedimetric sensor specificity, the cross-reactivity of the sensor (1:1 diluted SU, Gly 5×10^{-5} mol L^{-1}) under optimal conditions was recorded. The EIS responses of the fabricated sensors in the presence of glucose, ascorbic acid and caffeine (all present in the same concentration of 5 mmol L^{-1}) were taken and chosen according to a literature survey (Table s6). The change of C_{eff} was evaluated as the ratio between the values of C_{eff}, in the presence and absence of a specific interfering molecule. As shown in Table 2, the cross-reactivity for glucose, ascorbic acid and caffeine were less than 1 % and 5 % for the qBCNW and sBCNW, respectively.

In addition, the five consecutive detections (target concentration of Gly equal to 10^{-6} mol L^{-1}) were analyzed to investigate the stability of developed sensors. Results are reported in Table S3, highlighting that the analytical performance was quite stable (with the standard deviation, SD, below 5 %) for several consecutive analyses.

3.5. Molecular dynamic simulation of DFO derivatives adsorption at the electrode surface

The conducted MD simulations made it possible to compare the adsorption energies of the DFO derivatives at the TiO_2 electrode formed during the glycine determination process [34]. The CNW substrate was neglected in the analysis since the exposed electrode surface is composed of DFO@TiO_2 film. The nanocarbon structure functions mainly as a current collector encapsulated by a TiO_2 matrix. The adsorption energy E_{AD} was estimated at the equilibrated distance between molecules and the Tio_2 surface utilizing (7) [35]:

$$E_{AD} = E_{TOTAL} - E_{DFOD} - E_{TiO2}, \quad (7)$$

where, E_{TOTAL} represents the total energy of the system with the adsorbed derivatives, E_{DFOD} stands for the DFO derivatives energy, and E_{TiO2} is the energy of the pristine TiO_2.

The E_{AD} estimated for: (I) DFO, (II) DFO/glycine complex and (III) reference glycine representing α-amino acid was particularly studied. The distance of molecule – TiO_2 – for the listed cases was investigated by performing equilibration of three distinct orientations of molecules at the titania surfaces as shown in Fig. S8 and summarized in Table S7.

The optimal distances with the lowest adsorption energies were equal to 1.77 Å, 1.90 Å and 1.54 Å for the (I), (II) and (III) cases, respectively. The E_{AD} of the DFO/glycine complex is approx. 25 % lower than the adsorption values of DFO or pristine glycine, revealing the high efficiency and sensitivity of the proposed system. Such an effect could be attributed to intense chemisorption in contrast to the weak physical interaction of the physisorbed molecules [17,36,37]. The lower the distance between the TiO_2 surface and the closest atoms of the adsorbate, the higher the affinity for chemisorption in the case of (II) the DFO-glycine complex. Monti et al. [38] showed that outer amino acid layers were not able to be incorporated into the densely packed TiO_2 matrix. The obtained MD results showed that higher E_{AD} values of the DFO/glycine complex indicated effective chemisorption, therefore the complexed DFO/glycine derivatives are formed at the TiO_2 surface. This confirms that detection is induced by the presence of DFO in the TIO_2 matrix, while glycine will be suppressed from pristine TiO_2 gel since its rection with DFO is energetically preferred. 1,8-diazafluoren-9-one forms a highly efficient fluorescent complex with α-amino acids to form structurally stable complexes similar to ninhydrin (see Fig. 6a) [36]. The adhesion forces could be characterized by the adsorption energy, which was calculated from the energy differences of the states optimized in terms of the adsorbed and desorbed geometries. Slightly higher values were obtained for glycine adsorbed at crystalline forms of TiO_2, than those obtained in our study – 118.28 kJ/mol for nanocrystalline rutile. For glycine simulated at crystalline (110) rutile [39], a value of 161 kJ/mol was reported if the carboxyl group was bound to the surface. With the addition of a hydrogen bond from the amino group to the bridging oxygen atom, the energy increased to 197 kJ/mol, which indicates that the adsorption energy is mainly attributed to the carboxyl group [39].

Table 2
Effect of interfering species.

Species	Concentration	Molecular weight	Change of C_{eff}	
			sBCNW/ DFO@TiO_2	qBCNW/ DFO@TiO_2
Glucose	5 μM	180.16 g/ mol	(97.4 ± 3.0) %	(100 ± 0.1) %
Ascorbic acid	5 μM	176.12 g/ mol	(103.1 ± 5.5) %	(99.8 ± 0.2) %
Caffeine	5 μM	194.19 g/ mol	(99.0 ± 5.6) %	(100.6 ± 0.2) %

* The results are expressed as mean ± mean absolute error (n = 3).

3.6. Suggested sensing mechanism

BCNWs is a p-type semiconductor, with an estimated bandgap of approximately ≈ 0.15–0.2 eV, which decreases as the sample thickness increases and eventually approaches zero [40,41]. Amorphous TiO_2 is an n-type semiconductor, with an estimated bandgap of 3.1 eV [42]. According to Fig. 6a, when α-amino acids such as glycine react with the DFO within the amorphous TiO_2-gel, firstly, an imine is formed, which undergoes decarboxylation and hydrolysis to form an aromatic amine. Then, the latter one reacts further with an excess of DFO to form the reaction product, as highlighted in yellow [15], which can be rearranged accordingly [37]. A direct comparison of the lowest adsorption configurations is shown in Fig. 6b. Thus, the biochemical reactions induce an electrical charge at the insulating interface, resulting in the variation of the space charge capacitance (Fig. 6c), as also highlighted by the PLS analysis (ROI2). For this reason, only the DFO at the interface is responsible for the sensing mechanism, but the different BCNW layers affect it in two ways: directly, by increasing surface area which results in a lower ΔE_p and lower surface resistivity, and indirectly, because of the different DFO@TiO_2 interfacial morphology (Fig. 2c,d). However, since the detection mechanism is ruled by the change of the lowest capacitance in series, it is therefore important that the capacitance in the insulating layer is as high as possible, otherwise, it may not dominate, and analyte changes might not be detectable [43]. For this reason, in the TiO_2-insulating layer, the micropattern formed on qBCNW is more uniform, but DFO is unevenly dispersed on the surface, resulting in lower sensitivity and SD (thus, LoD).

On the other hand, DFO is uniformly dispersed on the sBCNW surface, resulting in higher sensitivity, but due to the higher density of cavities, in which the insulating layer appears thinned (Fig. 2), the precision decreases, resulting in a higher LoD. The homogeneity factor (α), of the CPE element, well describes the presence of defects on the coating surface [44]. Moreover, due to the shorter BCNW layer thickness in the qBCNW electrode, the limited availability of charge carriers results in a one-order magnitude smaller space charge capacitance. By applying a potential greater than or equal to 0 V, to the electrode, the charge transfer resistance increases with the increasing Gly concentration, while it decreases when a negative potential is applied (Fig. 3,c,d). This aspect can be explained by the positively charged DFO reaction product which hinders the ion mobility toward the electrode, while it facilitates when the electrode is negatively polarized (Fig. 6c). Moreover, Han et al. [45] reported that a mixed phase TiO_2/diamond heterojunction electrode exhibits high photoelectrocatalytic activity and

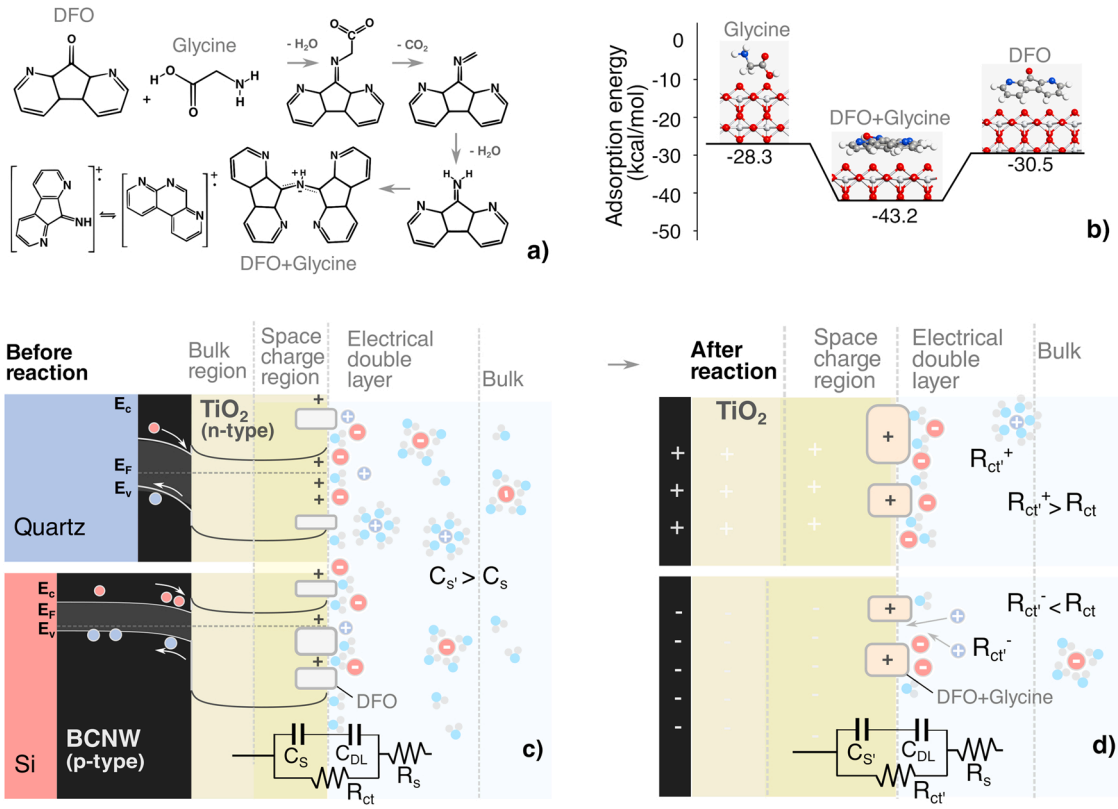

Fig. 6. (a) Proposed sensing mechanism based on the DFO reaction with glycine. (b) Energy diagram calculated by the DFT method. Detection mechanism schematic (c) before and (d) after the reaction of DFO with α-amino acids.

stability across a wide pH range, allowing for enhanced detection of organic compounds. Yuan et al. [46] revealed high separation of generated charge carriers in the titania/diamond junctions with low loss of activity. TiO_2 layer deposition on a boron-doped diamond surface was studied by Behúl [47] forming a p-n junction electrochemical electrode with improved hole injection from BDD, since many more electrons and holes are recombined during redox reactions. A non-exhaustive list of electrochemical sensors for the detection of specific amino acids is reported in Table 3.

4. Conclusions

In this study, we developed a non-faradaic electrochemical impedimetric biosensor for the determination of α-amino acids. The developed biosensing probe exhibits specific reactivity with α-amino acids, due to the DFO, and superior charge transfer by using BCNW as a transducer. The heterostructures revealed a unique maze-like morphology supported by Ti-rich boundary micelles delivering synergistically excellent semiconducting performance as shown by Mott-Schottky analyses. The hypothesized sensing mechanism of the organic molecule- α-amino acid-detection is based on the surficial adsorption forming DFO derivatives aligning the Fermi energy level of a p-type semiconducting electrode. The changes of capacitance recorded during the reaction of the DFO-rich electrode with the glycine achieved a limit of detection as low as 0.62 μM along with a large linear readout in the logarithmic range of glycine in PS from 0.1 to 1000 μM. In addition, the electrochemically impedimetric process was investigated by PLS, without the need for fitting the EIS spectra to an EEC. PLS models highlighted the presence of

Table 3
Overview of reported electrode materials for the electrochemical detection of amino acids.

Sensor	Analyte (s) *	Detection technique	Concentration range (μM)	LoD (μM)	Ref
Screen-printed glycine oxidase-based electrode	Gly	Amp		11	[1]
Ruthenium hexacyanoferrate/reduced graphene oxide electrode	Glu, Th, Gly	SWV	1.25–7.49 (Gly)	0.4 (Gly)	[48]
Glassy carbon electrode modified with nickel oxide nanoparticles	Gly, L-Ser, L-Al	Amp	1–200 (Gly) 1–400 (Ser) 30–200 (L-al)	0.9 (Gly) 0.85 (Ser) 29.67 (L-Al)	[49]
Multiwall carbon nanotubes/Fe (III)–Schiff base complex	Val, L-Phe, L-Arg, Gly, Ser, Tyr, L-Trp	DPV	3–12200 (Gly) 20–1200 (L-Trp) 9–5000 (L-Phe)	4.11 (Gly) 1.1 (L-Trp) 13.7 (L-Phe)	[50]
Silver oxide nanoparticles/reduced graphene oxide modified electrode	Gly, L-Al, Leu, Asp, Glu	Amp	10–1000	7.9 (Gly) 8.7 (Alan)	[51]
Current study	Gly, Try, Phe, Sar	EIS	0.05–1000	0.05 (Gly)	

* Analytes: Gly: glycine, Th: threonine, Glu: glutathione, L-ser: L-Serine, L-Al: L-Alanine, Val: valine, L-Phe: L- Phenylalanine,L-Ar: L-Arginine, L-TRP: L-Tryptophan, Leu; leucine, Asp: aspartic acid, Glu: glutamic acid. Detection methods: Amp: Amperometric, SWV: Square Wave Voltammetry, DPV: Differential Pulse Voltammetry, EIS: Electrochemical impedance spectroscopy.

two ROIs, pointing out the modification of the space charge capacitance as a consequence of the increasing Gly concentration. Similarly, the conducted MD simulations supported the experimental data, showing large differences in adsorption energies of DFO derivatives at the TiO_2 electrode formed during the glycine determination process. The DFO/glycine complex revealed a more than 25 % lower adsorption energy than DFO or pristine glycine, revealing the high efficiency and sensitivity of the proposed system. Such effect was attributed to intensive chemisorption of Gly to the electrode. Moreover, the heterostructure resulted in high cross-sensitivity versus other α-amino acids (i.e. tryptophan and sarcosine) and cross-selectivity versus other amino acids (i.e. β-alanine and taurine). The developed heterostructures could be applied for further statistical investigations of the behavior of α-amino acids in different clinical samples (i.e. blood serum).

CRediT authorship contribution statement

Mattia Pierpaoli: Conceptualization, Methodology, Software, Formal analysis, Investigation, Data curation, Writing – original draft, Visualization, Writing – review & editing. **Aneta Lewkowicz:** Conceptualization, Methodology, Formal analysis, Investigation, Resources, Data curation, Writing – original draft. **Bartłomiej Dec:** Methodology, Software, Formal analysis, Data curation, Writing – original draft. **Małgorzata Nadolska:** Investigation, Data curation, Writing – original draft. **Robert Bogdanowicz:** Resources, Writing – review & editing, Supervision, Project administration.

Declaration of Competing Interest

The authors declare that they have no known competing financial interests or personal relationships that could have appeared to influence the work reported in this paper.

Data Availability

Data will be made available on request.

Acknowledgement

Financial support of these studies from Gdańsk University of Technology under the Nobelium - 'Excellence Initiative - Research University' program (M. Pierpaoli) and by the grant 2021/41/B/HS5/03250 of the National Science Centre (A. Lewkowicz) are gratefully acknowledged.

Appendix A. Supporting information

Supplementary data associated with this article can be found in the online version at doi:10.1016/j.snb.2022.132459.

References

[1] Q. Wang, Y. Liu, J.C. Campillo-Brocal, A. Jiménez-Quero, G.A. Crespo, M. Cuartero, Electrochemical biosensor for glycine detection in biological fluids, Biosens. Bioelectron. 182 (2021), 113154, https://doi.org/10.1016/j.bios.2021.113154.

[2] R.K. Murray, D.K. Granner, P.A. Mayes, V.W. Rodwell, Harper's Illustrated Biochemistry, Mcgraw-hill, 2014.

[3] A. Sreekumar, L.M. Poisson, T.M. Rajendiran, A.P. Khan, Q. Cao, J. Yu, B. Laxman, R. Mehra, R.J. Lonigro, Y. Li, M.K. Nyati, A. Ahsan, S. Kalyana-Sundaram, B. Han, X. Cao, J. Byun, G.S. Omenn, D. Ghosh, S. Pennathur, D.C. Alexander, A. Berger, J. R. Shuster, J.T. Wei, S. Varambally, C. Beecher, A.M. Chinnaiyan, Metabolomic profiles delineate potential role for sarcosine in prostate cancer progression, Nature 457 (2009) 910–914, https://doi.org/10.1038/nature07762.

[4] C. Pérez-Ràfols, Y. Liu, Q. Wang, M. Cuartero, G.A. Crespo, Why not glycine electrochemical biosensors? Sens. (Switz.) 20 (2020) 1–19, https://doi.org/10.3390/s20144049.

[5] M. Adeva-Andany, G. Souto-Adeva, E. Ameneiros-Rodríguez, C. Fernández-Fernández, C. Donapetry-García, A. Domínguez-Montero, Insulin resistance and glycine metabolism in humans, Amino Acids 50 (2018) 11–27.

[6] D.A. Applegarth, J.R. Toone, Nonketotic hyperglycinemia (glycine encephalopathy): laboratory diagnosis, Mol. Genet. Metab. 74 (2001) 139–146.

[7] M.H. Mahbub, N. Yamaguchi, H. Takahashi, R. Hase, H. Amano, M. Kobayashi-Miura, H. Kanda, Y. Fujita, H. Yamamoto, M. Yamamoto, Alteration in plasma free amino acid levels and its association with gout, Environ. Health Prev. Med. 22 (2017) 1–7.

[8] P. Krumpochova, B. Bruyneel, D. Molenaar, A. Koukou, M. Wuhrer, W.M. A. Niessen, M. Giera, Amino acid analysis using chromatography–mass spectrometry: An inter platform comparison study, J. Pharm. Biomed. Anal. 114 (2015) 398–407.

[9] V. Brabec, V. Mornstein, Electrochemical behaviour of proteins at graphite electrodes: II. Electrooxidation of amino acids, Biophys. Chem. 12 (1980) 159–165, https://doi.org/10.1016/0301-4622(80)80048-2.

[10] E.V. Suprun, E.V. Karpova, S.P. Radko, A.A. Karyakin, Advanced electrochemical detection of amino acids and proteins through flow injection analysis and catalytic oxidation on Prussian Blue, Electrochim. Acta 331 (2020), 135289, https://doi.org/10.1016/j.electacta.2019.135289.

[11] L. Syedmoradi, M.L. Norton, K. Omidfar, Point-of-care cancer diagnostic devices: from academic research to clinical translation, Talanta 225 (2021), 122002, https://doi.org/10.1016/j.talanta.2020.122002.

[12] M. Brodowski, M. Kowalski, M. Skwarecka, K. Pałka, M. Skowicki, A. Kula, T. Lipiński, A. Dettlaff, M. Ficek, J. Ryl, K. Dziąbowska, D. Nidzworski, R. Bogdanowicz, Highly selective impedimetric determination of Haemophilus influenzae protein D using maze-like boron-doped carbon nanowall electrodes, Talanta 221 (2021), 121623, https://doi.org/10.1016/j.talanta.2020.121623.

[13] K. Siuzdak, M. Ficek, M. Sobaszek, J. Ryl, M. Gnyba, P. Niedziałkowski, N. Malinowska, J. Karczewski, R. Bogdanowicz, Boron-enhanced growth of micron-scale carbon-based nanowalls: a route toward high rates of electrochemical biosensing, ACS Appl. Mater. Interfaces 9 (2017) 12982–12992, https://doi.org/10.1021/acsami.6b16860.

[14] M. Pierpaoli, M. Ficek, M. Rycewicz, M. Sawczak, J. Karczewski, M. Ruello, R. Bogdanowicz, M. Pierpaoli, M. Ficek, M. Rycewicz, M. Sawczak, J. Karczewski, M.L. Ruello, R. Bogdanowicz, Tailoring electro/optical properties of transparent boron-doped carbon nanowalls grown on quartz, Mater. (Basel) 12 (2019) 547, https://doi.org/10.3390/ma12030547.

[15] A. Lewkowicz, R. Bogdanowicz, P. Bojarski, M. Pierpaoli, I. Gryczyński, A. Synak, M. Mońka, J. Karczewski, W. Struck-Lewicka, R. Wawrzyniak, The luminescence of 1, 8-Diazafluoren-9-one/titanium dioxide composite thin films for optical application, Mater. (Basel) 13 (2020) 3014.

[16] A. Lewkowicz, K. Baranowska, P. Bojarski, M. Józefowicz, Solvent dependent spectroscopic properties of fingerprint reagent - 1,8-Diazafluoren-9-one, J. Mol. Liq. 285 (2019) 754–765, https://doi.org/10.1016/j.molliq.2019.04.110.

[17] D. Wilkinson, Study of the reaction mechanism of 1,8-diazafluoren-9-one with the amino acid, L-alanine, Forensic Sci. Int. 109 (2000) 87–103, https://doi.org/10.1016/S0379-0738(99)00219-4.

[18] P. Geladi, A. Nelson, B. Lindholm-Sethson, Complex numbers in chemometrics. Examples from multivariate impedance measurements on lipid monolayers, Anal. Chim. Acta 595 (2007) 152–159, https://doi.org/10.1016/j.aca.2007.01.037.

[19] D.R. Rodrigues, A.C. Olivieri, W.D. Fragoso, S.G. Lemos, Complex numbers-partial least-squares applied to the treatment of electrochemical impedance spectroscopy data, Anal. Chim. Acta 1080 (2019) 1–11, https://doi.org/10.1016/j.aca.2019.07.047.

[20] M. Pierpaoli, M. Ficek, P. Jakobczyk, J. Karczewski, R. Bogdanowicz, Self-assembly of vertically oriented graphene nanostructures: multivariate characterisation by Minkowski functionals and fractal geometry, Acta Mater. (2021), 116989, https://doi.org/10.1016/j.actamat.2021.116989.

[21] M. Sobaszek, K. Siuzdak, J. Ryl, M. Sawczak, S. Gupta, S.B. Carrizosa, M. Ficek, B. Dec, K. Darowicki, R. Bogdanowicz, Diamond phase (sp3-C) rich boron-doped carbon nanowalls (sp2-C): physicochemical and electrochemical properties, J. Phys. Chem. C. 121 (2017) 20821–20833, https://doi.org/10.1021/acs.jpcc.7b06365.

[22] A. Lewkowicz, M. Kantor, W. Zalewski, P. Bojarski, M. Mońka, Spectroscopic evidence of fluorescence by 1,8–diazafluoren-9–one aggregates—A prospective new ultrasensitive method for fingerprint trace detection, J. Forensic Sci. (2022) 1–8, https://doi.org/10.1111/1556-4029.15039.

[23] B.S. Henson, D.T. Wong, Collection, storage, and processing of saliva samples for downstream molecular applications, Methods Mol. Biol. 666 (2010) 21–30, https://doi.org/10.1007/978-1-60761-820-1_2.

[24] T. Brooks, C.W. Keevil, A simple artificial urine for the growth of urinary pathogens, Lett. Appl. Microbiol. 24 (1997) 203–206, https://doi.org/10.1046/j.1472-765X.1997.00378.x.

[25] D.A. Armbruster, T. Pry, Limit of blank, limit of detection and limit of quantitation, Clin. Biochem. Rev. 29 (Suppl 1) (2008) S49–52. ⟨http://www.ncbi.nlm.nih.gov/pubmed/18852857%0Ahttp://www.pubmedcentral.nih.gov/articlerender.fcgi?artid=PMC2556583⟩.

[26] S. Kucheryavskiy, mdatools–R package for chemometrics, Chemom. Intell. Lab. Syst. 198 (2020), 103937.

[27] R. Core Team, R: A language and environment for statistical computing., (2013).

[28] J. Schneider, J. Hamaekers, S.T. Chill, S. Smidstrup, J. Bulin, R. Thesen, A. Blom, K. Stokbro, ATK-ForceField: a new generation molecular dynamics software package, Model. Simul. Mater. Sci. Eng. 25 (2017), https://doi.org/10.1088/1361-651X/aa8ff0.

[29] S. Monti, V. Carravetta, H. Ågren, Simulation of gold functionalization with cysteine by reactive molecular dynamics, J. Phys. Chem. Lett. 7 (2016) 272–276, https://doi.org/10.1021/acs.jpclett.5b02769.

[30] C. Ashraf, A.C.T.Van Duin, Extension of the ReaxFF combustion force field toward syngas combustion and initial oxidation kinetics, J. Phys. Chem. A. 121 (2017) 1051–1068, https://doi.org/10.1021/acs.jpca.6b12429.
[31] G.J. Brug, A.L.G. van den Eeden, M. Sluyters-Rehbach, J.H. Sluyters, The analysis of electrode impedances complicated by the presence of a constant phase element, J. Electroanal. Chem. 176 (1984) 275–295, https://doi.org/10.1016/S0022-0728(84)80324-1.
[32] B. Hirschorn, M.E. Orazem, B. Tribollet, V. Vivier, I. Frateur, M. Musiani, Determination of effective capacitance and film thickness from constant-phase-element parameters, Electrochim. Acta 55 (2010) 6218–6227, https://doi.org/10.1016/j.electacta.2009.10.065.
[33] O.Y. Rodionova, A.L. Pomerantsev, Detection of outliers in projection-based modeling, Anal. Chem. 92 (2020) 2656–2664, https://doi.org/10.1021/acs.analchem.9b04611.
[34] S. Ebrahimi Loushab, M.R. Benam, R.P. Shahri, J. Baedi, A. Feyzi, Investigation of the phosphorene nano-sheet as a sensor for detecting aspartic-acid, alanine and glycine amino acids: a first principle study, Phys. B Condens. Matter 618 (2021), 412771, https://doi.org/10.1016/j.physb.2020.412771.
[35] Y. Du, H. Liu, B. Xu, L. Sheng, J. Yin, C.G. Duan, X. Wan, Unexpected magnetic semiconductor behavior in zigzag phosphorene nanoribbons driven by half-filled one dimensional band, Sci. Rep. 5 (2015) 1–5, https://doi.org/10.1038/srep08921.
[36] O. Petrovskaia, B.M. Taylor, D.B. Hauze, P.J. Carroll, M.M. Joullié, Investigations of the reaction mechanisms of 1,2-indanediones with amino acids, J. Org. Chem. 66 (2001) 7666–7675, https://doi.org/10.1021/jo0105179.
[37] R. Grigg, T. Mongkolaussavaratana, C. Anthony Pounds, S. Sivagnanam, 1,8-diazafluorenone and related compounds. A new reagent for the detection of (α-amino acids and latent fingerprints, Tetrahedron Lett. 31 (1990) 7215–7218, https://doi.org/10.1016/S0040-4039(00)97283-6.
[38] S. Monti, A.C.T. van Duin, S. Kim, V. Barone, Exploration of the conformational and reactive dynamics of glycine and diglycine on TiO 2: computational investigations in the gas phase and in solution, J. Phys. Chem. C. 116 (2012) 5141–5150, https://doi.org/10.1021/jp2121593.
[39] S. Köppen, O. Bronkalla, W. Langel, Adsorption configurations and energies of amino acids on anatase and rutile surfaces, J. Phys. Chem. C. 112 (2008) 13600–13606, https://doi.org/10.1021/jp803354z.
[40] M. Ficek, B. Dec, K.J. Sankaran, K. Gajewski, P. Tatarczak, I. Wlasny, A. Wysmolek, K. Haenen, T. Gotszalk, R. Bogdanowicz, Stable field electron emission and plasma illumination from boron and nitrogen Co-doped edge-rich diamond-enhanced carbon nanowalls, Adv. Mater. Interfaces 8 (2021), https://doi.org/10.1002/admi.202100464.
[41] S. Kawai, S. Kondo, W. Takeuchi, H. Kondo, M. Hiramatsu, M. Hori, Optical properties of evolutionary grown layers of carbon nanowalls analyzed by spectroscopic ellipsometry, Jpn. J. Appl. Phys. 49 (2010) 0602201–0602203, https://doi.org/10.1143/JJAP.49.060220.
[42] A. Lewkowicz, A. Synak, B. Grobelna, R. Bogdanowicz, J. Karczewski, K. Szczodrowski, M. Behrendt, Thickness and structure change of titanium(IV) oxide thin films synthesized by the sol–gel spin coating method, Opt. Mater. (Amst.). 36 (2014) 1739–1744, https://doi.org/10.1016/J.OPTMAT.2014.02.033.
[43] C. Berggren, B. Bjarnason, G. Johansson, Capacitive biosensors, Electroanalysis 13 (2001) 173–180, https://doi.org/10.1002/1521-4109(200103)13:3<173::AID-ELAN173>3.0.CO;2-B.
[44] J. Vogelsang, W. Strunz, The evaluation of experimental dielectric data of barrier coatings by means of different models, Electrochim. Acta 46 (2001) 3619–3625, https://doi.org/10.1016/S0013-4686(01)00644-2.
[45] Y. Han, X. Ruan, J. Chen, H. Zhang, H. Zhao, S. Zhang, Photoelectrochemical properties and its application of nano-tio 2/boron-doped diamond heterojunction electrode material, Asian J. Chem. 25 (2013) 6167–6172, https://doi.org/10.14233/ajchem.2013.14299.
[46] J. Yuan, H. Li, S. Gao, Y. Lin, H. Li, A facile route to n-type TiO2-nanotube/p-type boron-doped-diamond heterojunction for highly efficient photocatalysts, Chem. Commun. 46 (2010) 3119–3121, https://doi.org/10.1039/c003172k.
[47] M. Behúl, M. Vojs, M. Marton, P. Michniak, M. Mikolášek, M. Kurniawan, H. L. Honig, D.V. Zyabkin, M.O. Ramirez, L. Spieß, D. Flock, A. Bund, M. Papula, R. Redhammer, Nanostructured boron doped diamond enhancing the photoelectrochemical performance of TiO2/BDD heterojunction anodes, Vacuum 171 (2020), 109006, https://doi.org/10.1016/j.vacuum.2019.109006.
[48] S. Saranya, J. Jency Feminus, B. Geetha, P.N. Deepa, Simultaneous detection of glutathione, threonine, and glycine at electrodeposited RuHCF/rGO–modified electrode, Ion. (Kiel.) 25 (2019) 5537–5550, https://doi.org/10.1007/s11581-019-03064-8.
[49] M. Roushani, M. Shamsipur, S.M. Pourmortazavi, Amprometric detection of Glycine, L-Serine, and L-Alanine using glassy carbon electrode modified by NiO nanoparticles, J. Appl. Electrochem 42 (2012) 1005–1011, https://doi.org/10.1007/s10800-012-0475-4.
[50] L. Saghatforoush, M. Hasanzadeh, N. Shadjou, B. Khalilzadeh, Deposition of new thia-containing Schiff-base iron (III) complexes onto carbon nanotube-modified glassy carbon electrodes as a biosensor for electrooxidation and determination of amino acids, Electrochim. Acta 56 (2011) 1051–1061, https://doi.org/10.1016/j.electacta.2010.10.031.
[51] V.H.R. Azevedo, J.L. da Silva, N.R. Stradiotto, Silver oxide nanoparticles in reduced graphene oxide modified electrode for amino acids electrocatalytic oxidation, J. Electroanal. Chem. 845 (2019) 57–65, https://doi.org/10.1016/j.jelechem.2019.05.037.

Mattia Pierpaoli main interests and competencies lie in the field of advanced carbon nanomaterials for environmental applications and sensing. In 2019 he was awarded the PhD title, after being visiting PhD student at the Gdansk University of Technology (Poland) and Shanghai Jiao Tong University (China). He is currently conducting Research on CVD-grown three-dimensional carbon nanomaterials at the Gdańsk University of Technology, where he holds the position as associate professor.

Aneta Lewkowicz is an assistant professor at University of Gdańsk. She awarded her PhD in Physics, in the field of molecular spectroscopy and forensic science. She has documented experience on structural-spectroscopic analysis of compounds used in forensic science, such as hybrid nanofilms, thin films, and bulk.

Bartłomiej Dec, is a PhD student at the Faculty of Electronics, Telecommunications and Informatics of Gdansk University of Technology. His main interests are parallel programming and source code optimization combined with electronic control systems in the fields of modern electronic and optoelectronic materials. Scientific interests include quantum computing and molecular dynamics.

Małgorzata Nadolska is a PhD student at Gdańsk University of Technology in the Institute of Nanotechnology and Materials Engineering. Her research interests include functionalized carbon materials and surface analysis, in particular spectroscopy techniques and adsorption phenomena.

Robert Bogdanowicz received his Ph.D. degree (with distinction) in Electronics from the Gdansk University of Technology in 2009. His current domains of interest include selective CVD diamond growth and nanocrystalline diamond doping for environmental and biochemical nanosensors. In 2015 he held a scholarship Fulbright Senior Scholar Program at the California Institute of Technology (Caltech) in the group of prof. William Goddard (Materials and Process Simulation Center) working on hybrid 3D diamond structures.